



RESEARCH LETTER

10.1002/2015GL067173

Key Points:

- LFEs have slow rupture and slip velocities
- LFEs are low stress drop events (~10 kPa)
- Seismic and aseismic components of slow slip can be explained by the same mechanism

Correspondence to:

A. M. Thomas,
amthomas@uoregon.edu

Citation:

Thomas, A. M., G. C. Beroza, and D. R. Shelly (2016), Constraints on the source parameters of low-frequency earthquakes on the San Andreas Fault, *Geophys. Res. Lett.*, 43, doi:10.1002/2015GL067173.

Received 24 NOV 2015

Accepted 22 JAN 2016

Accepted article online 28 JAN 2016

Constraints on the source parameters of low-frequency earthquakes on the San Andreas Fault

Amanda M. Thomas¹, Gregory C. Beroza², and David R. Shelly³

¹Department of Geological Sciences, University of Oregon, Eugene, Oregon, USA, ²Department of Geophysics, Stanford University, Stanford, California, USA, ³U.S. Geological Survey, Menlo Park, California, USA

Abstract Low-frequency earthquakes (LFEs) are small repeating earthquakes that occur in conjunction with deep slow slip. Like typical earthquakes, LFEs are thought to represent shear slip on crustal faults, but when compared to earthquakes of the same magnitude, LFEs are depleted in high-frequency content and have lower corner frequencies, implying longer duration. Here we exploit this difference to estimate the duration of LFEs on the deep San Andreas Fault (SAF). We find that the $M \sim 1$ LFEs have typical durations of ~ 0.2 s. Using the annual slip rate of the deep SAF and the average number of LFEs per year, we estimate average LFE slip rates of ~ 0.24 mm/s. When combined with the LFE magnitude, this number implies a stress drop of $\sim 10^4$ Pa, 2 to 3 orders of magnitude lower than ordinary earthquakes, and a rupture velocity of 0.7 km/s, 20% of the shear wave speed. Typical earthquakes are thought to have rupture velocities of ~ 80 – 90% of the shear wave speed. Together, the slow rupture velocity, low stress drops, and slow slip velocity explain why LFEs are depleted in high-frequency content relative to ordinary earthquakes and suggest that LFE sources represent areas capable of relatively higher slip speed in deep fault zones. Additionally, changes in rheology may not be required to explain both LFEs and slow slip; the same process that governs the slip speed during slow earthquakes may also limit the rupture velocity of LFEs.

1. Introduction

Low-frequency earthquakes (LFEs) are small repeating earthquakes that make up tectonic tremor and occur in conjunction with slow earthquakes [Shelly *et al.*, 2007; Ide *et al.*, 2007a, 2007b; Beroza and Ide, 2011]. LFEs have been observed predominantly in subduction zone settings [Shelly *et al.*, 2007; Brown *et al.*, 2013; Frank *et al.*, 2013; Royer and Bostock, 2014; Plourde *et al.*, 2015; Thomas and Bostock, 2015] and also occur on some continental faults [Shelly and Hardebeck, 2010; Chamberlain *et al.*, 2014]. Like typical earthquakes, LFEs are generated by shear slip, but when compared to earthquakes of similar magnitude, LFEs are depleted in high-frequency content and have lower corner frequencies, implying longer durations. On the Parkfield section of the San Andreas Fault, as in many subduction zones, LFEs occur in rapid succession forming tectonic tremor [Shelly *et al.*, 2007]. Shelly and Hardebeck [2010] identified and located 88 LFE families on the deep extension of the San Andreas between 16 and 29 km depth (Figure 1).

The seismogram of an earthquake contains information about the earthquake source, the structure through which the waves propagate, and the properties of the recording site. Isolating the contribution of the earthquake source to the observed seismogram requires removing propagation and site effects. Empirical Green's function (eGf) analysis is commonly employed to isolate the seismic source and involves using a second earthquake to remove common propagation effects from the target event [Hartzell, 1978; Mueller, 1985; Dreger *et al.*, 2007; Allmann and Shearer, 2007; Baltay *et al.*, 2014; Abercrombie, 2015]. There are three requirements that an eGf must satisfy: the eGf must be close to the target event such that their seismic waves traverse nearly the same path, the duration of the eGf must be short relative to the target event, and the two events must have similar focal mechanisms. If an earthquake pair satisfies these criteria, the eGf waveforms can be deconvolved from the target event waveforms resulting in the source time function or time history of fault slip for the target event, valid at frequencies below the corner frequency of the eGf event.

While eGf analysis may not seem suitable for studying the LFE source, using regular earthquakes that occur near the base of the seismogenic zone as eGfs for target LFEs can satisfy the three criteria outlined above. First, some of the shallowest LFE families have hypocenters within 3 km of the deepest regular earthquakes that occur beneath Parkfield. Studies of optimal eGf practices suggest that the eGf be no more than one rupture length away from the target event [Abercrombie, 2015]. That requirement is not satisfied by our data;

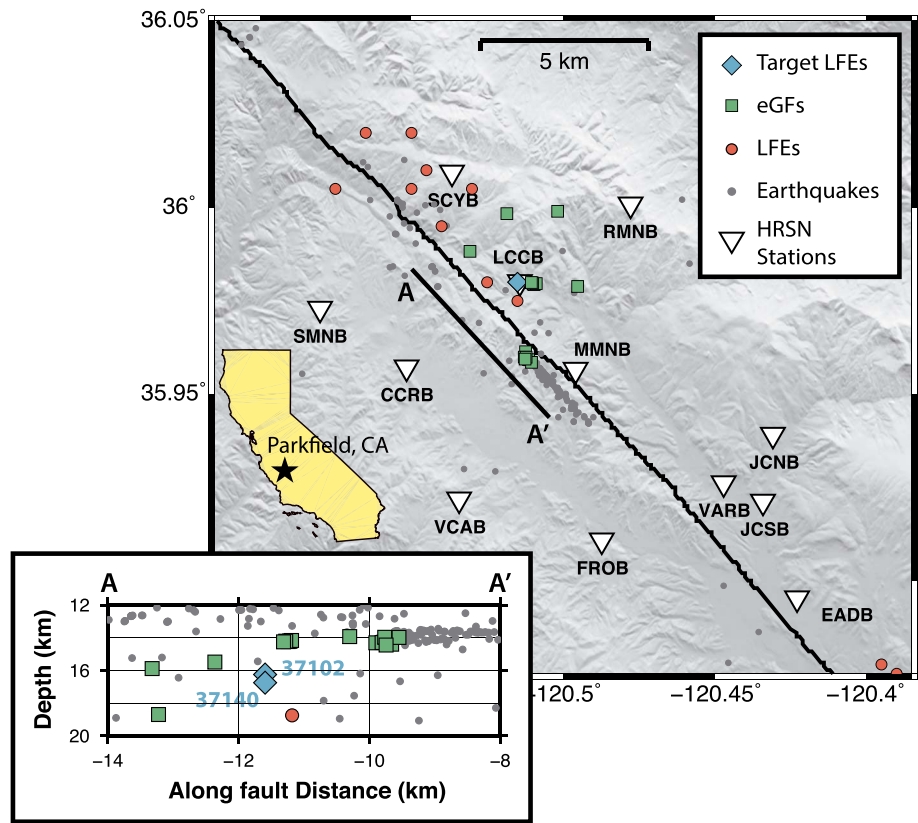


Figure 1. Map of the Parkfield, California area, HRSN borehole stations, and associated seismicity. LFEs identified by Shelly and Hardebeck [2010] are shown as red circles, relocated earthquakes below 12 km depth are shown in grey [Waldhauser and Schaff, 2008]. In this study we focus on the two target LFEs (blue squares) and eGFs (green circles). Inset in lower left shows earthquake locations in cross section (note 4 times vertical compression).

however, we mitigate its effect by using multiple eGFs for each target LFE (see section 2 for further details). Second, to use one of the deep earthquakes near Parkfield as an eGF for an LFE requires that the two events have substantially different durations so that the eGF approximates the earth response without a strong signature of its own source complexity. Precise magnitudes have not been determined for LFE sources in Parkfield; however, the amplitudes of body waves produced by the shallowest LFEs are consistent with M 1 events or smaller. While generally small in magnitude, most of the deep earthquakes are not below M 1; hence, for typical earthquakes, these events would not function as acceptable eGF candidates; however, LFEs are not typical earthquakes. cursory inspection of the LFE and eGF spectra (Figure 2) suggests that the two types of events have substantially different corner frequencies. Spectral falloff begins to occur between 4 and 5 Hz for the LFEs while the eGF spectra remain flat out to higher frequencies. Since corner frequency is thought to be inversely proportional to duration [Brune, 1970], the significant differences in corner frequency imply a significant difference in duration. This inferred difference in duration allows for more flexibility in the choice of eGF such that the deep $\sim M$ 1 earthquakes in Parkfield can be used effectively as eGFs for the nearby LFEs. Third, polarities of S wave arrivals of both the earthquakes and LFEs are in good agreement suggesting that the events have similar focal mechanisms. This conjecture is further supported by the observation that the small magnitude earthquakes used in this study are in close spatial proximity to larger earthquakes with right-lateral strike-slip focal mechanisms [Thurber et al., 2006]. Additionally, LFEs on the deep San Andreas have been shown to occur preferentially during times when tidal stresses encourage right-lateral shear slip [Thomas et al., 2012], suggesting that they also have strike-slip focal mechanisms.

Here we demonstrate that eGF analysis can be used to determine the average timescale of two different LFE families on the San Andreas Fault. We interpret this timescale as a rise time and calculate the stress drop and

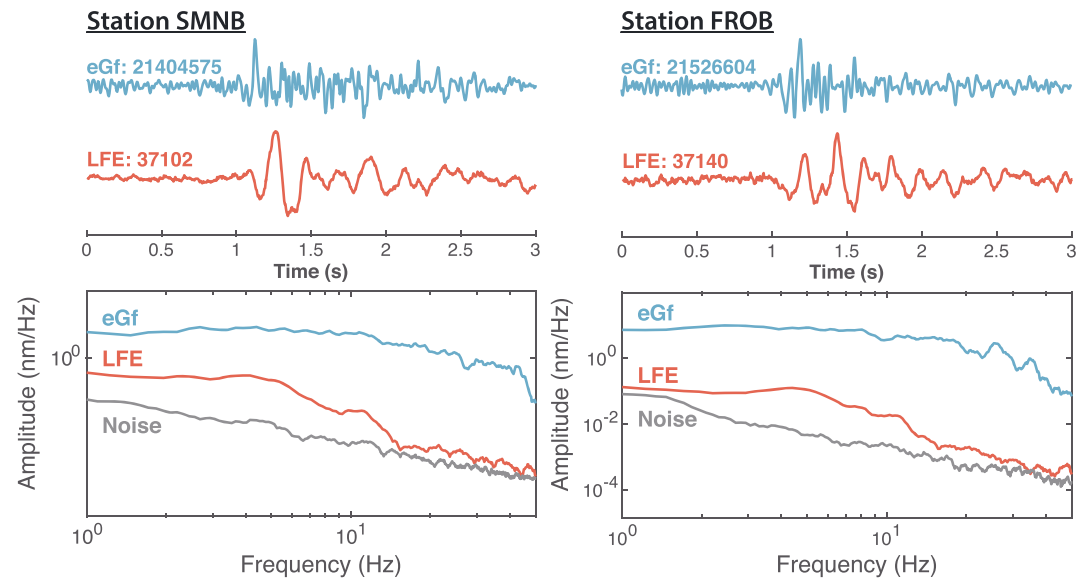


Figure 2. Example nearby earthquake (blue) and LFE (red) velocity waveforms and displacement spectra for stations SMNB and FROB. The stacked LFE records are used to obtain the source time functions shown in Figure 3. Waveforms are band-passed filtered between 1 and 50 Hz.

rupture velocity. We find that LFEs have stress drops, slip velocities, and rupture velocities that are much lower than those of typical earthquakes.

2. Methodology

We use borehole velocity seismograms from 12 stations from the High Resolution Seismic Network (HRSN) for eGf analysis of two different LFE families near Parkfield, CA (families 37102 and 37140, Figure 2). These families were chosen based on their close spatial proximity to multiple potential eGfs, and at each station and component we stack ~ 100 detections of each LFE family to increase the signal-to-noise ratios (SNR). For each family, we select all relocated earthquakes [Waldhauser and Schaff, 2008; Thurber et al., 2004] with hypocenters at a distance of less than 3 km from the respective LFE family and with catalog magnitudes of 1.4 or below. We also included two aftershocks of an M 2.1 event with a focal mechanism consistent with the local strike and dip of the San Andreas Fault. These selection criteria result in a total of 17 and 12 eGfs for family 37102 and 37140, respectively. We downloaded all waveform data from the Northern California Earthquake Data Center using the Simple Waveform Client, corrected for instrument response, and down-sampled to 100 Hz. We perform our analysis using S waves identified on horizontal components DP2 and DP3 filtered in the 1–50 Hz frequency band.

The eGf analysis typically involves deconvolving the eGf from the target event to recover the relative moment rate function. While we did experiment with this technique, it did not produce reliable estimates of duration due to the combination of low SNR in many of the eGfs and the band-limited nature of LFEs. Instead, for each eGf-LFE pair we convolve the eGf with a Hann window ($\alpha = 1$) with duration ranging from 0.01 to 1 s, meant to represent the LFE source time function, and then cross-correlate the resulting waveform with the LFE record. We chose a Hann window because it has shape and smoothness that closely resembles a Gaussian distribution but has the advantage of having a well-defined duration. We also employed boxcar source time functions and report results of both functional forms in section 3. We require that both the LFE and eGf have a SNR of greater than 3 to be included in our duration estimates. For each station and horizontal component, we compute the maximum cross-correlation coefficient between the LFE and synthetic seismogram as a function of duration. An example of this process for one eGf-LFE pair is shown in Figure 3. The cross-correlation versus duration curves are then averaged over all stations and components to produce a composite curve for each LFE-eGf pair (Figures 3b and 3c). Finally, we average the composite curves and estimate the duration of each LFE as the duration corresponding to the maximum average cross correlation.

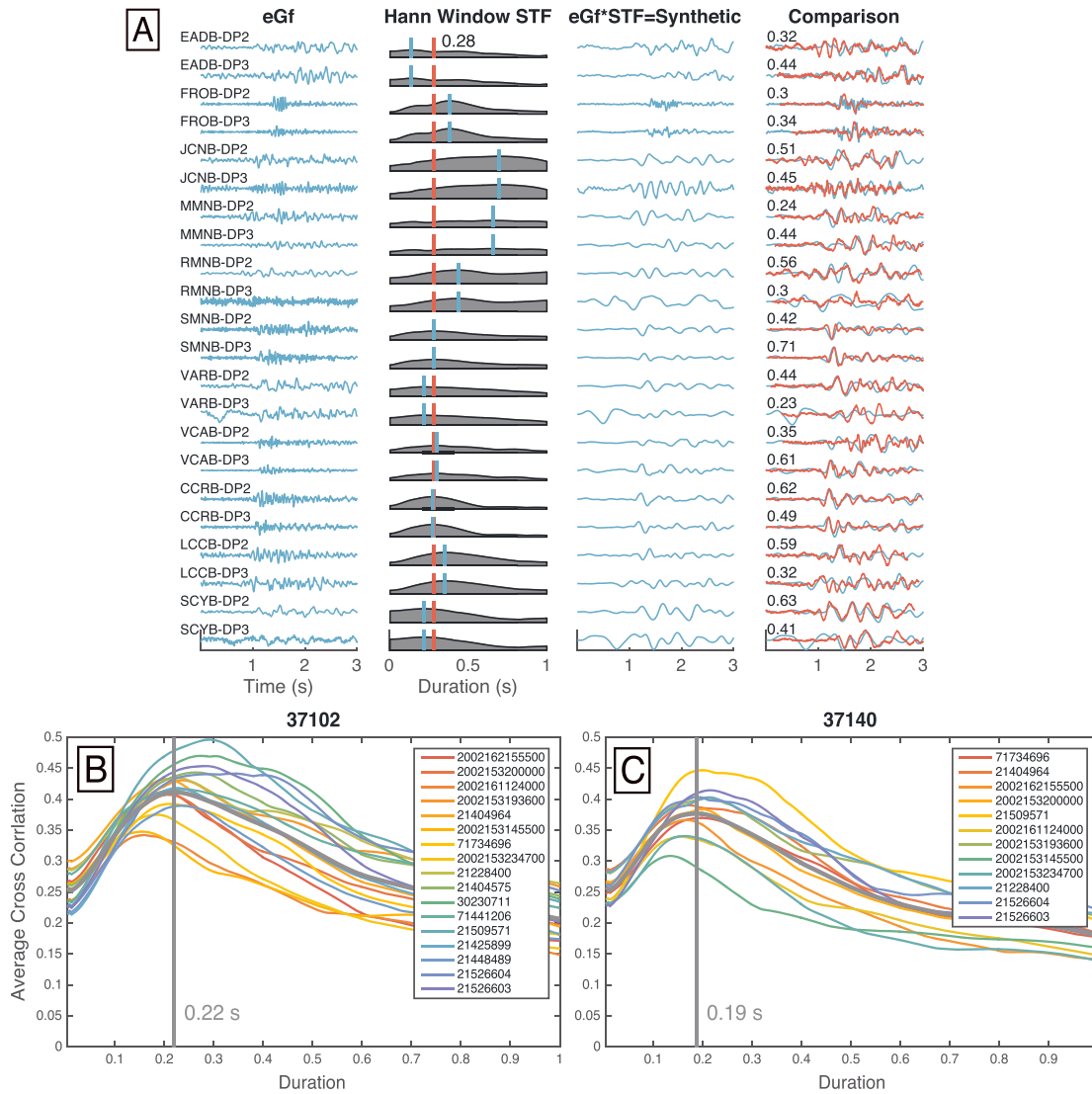


Figure 3. (a) Example of eGf convolution for a single LFE-eGf pair (LFE: 37102 and eGf: 21526603). First column shows eGf records for stations in the HRSN. The labels indicate the station and component shown. The second column shows the correlation coefficient of Hann window source time function with duration shown on the x axis convolved with the eGf (i.e., the synthetic seismogram) with the LFE waveform. The vertical blue line indicates the best fitting duration for each station (i.e., the maximum of the grey curve shown), while the red vertical line marks the overall best fitting duration (the duration that maximizes average cross-correlation coefficient over all stations and channels) for this particular eGf. The third column shows the convolution of the eGf and the source time function with the best fit duration for all stations (the red bar). The fourth column shows the comparison between the synthetic seismogram in the third column (blue) with the LFE waveform (red). Black numbers are cross-correlation coefficients between the eGf generated with the best fitting duration and the LFE waveforms. Average cross correlations as a function of duration for families (b) 37102 and (c) 37140. Curves are color coded by eGf and the mean cross-correlation value is indicated by the bold grey line. The maximum amplitude of the average cross-correlation curves are marked as vertical grey lines and correspond to 0.22 and 0.19 s for families 37102 and 37140, respectively.

3. Results

The average cross correlations as a function of duration for the two LFEs 37102 and 37140 are shown in Figures 3b and 3c. The average of the cross-correlation versus duration curves (using Hann window source time functions) over all eGfs (grey curve in Figures 3b and 3c) has a peak value corresponding to durations of 0.22 and 0.19 s for 37102 and 37140, respectively. These values are at least an order of magnitude greater than durations of typical *M* 1 earthquakes; however, they are similar to the ~0.5 s durations of LFEs in Cascadia [Bostock *et al.*, 2015]. The boxcar source time functions (not shown) resulted in durations of 0.11 and 0.08 s; however, we prefer the larger estimates for two reasons. First, the maximum average cross correlation is larger when using a Hann window source time function as opposed to a boxcar. Second, the ~0.2 s duration

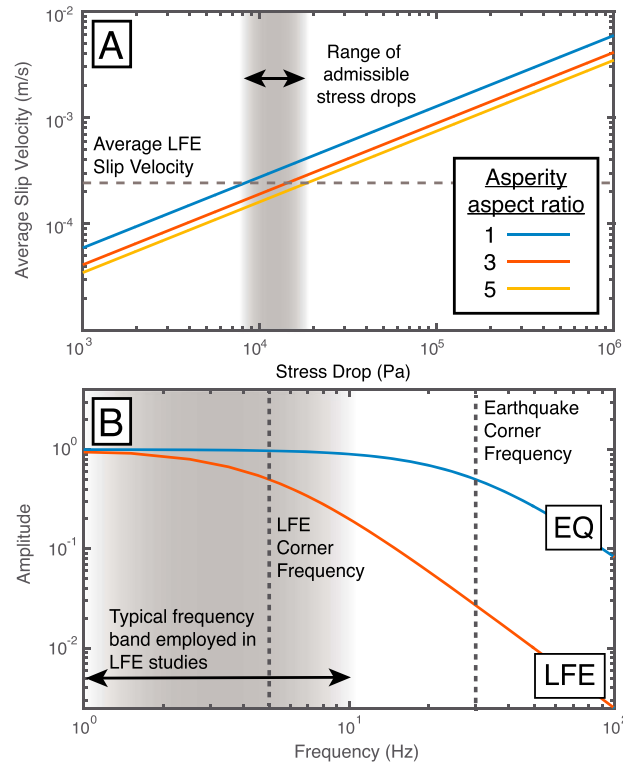


Figure 4. (a) The tradeoff between slip velocity and stress drop for a $M 1$ LFE. The estimated slip velocity using the long-term slip rate of the SAF is shown as a horizontal dashed line corresponding to a stress drop of ~ 10 kPa, for aspect ratios between 1 and 5. (b) The effect of changing the duration (i.e., the corner frequency) on the amplitude spectrum.

rupture the entire faulted surface). Because our analysis does not constrain the spatial extent of the LFE source, we cannot directly estimate the rupture velocity. If instead the LFE duration we measure represents the rise time, we can estimate the slip per LFE by taking the total slip rate on the deep SAF of 34 mm/yr [Ryder and Bürgmann, 2008] and dividing by the average number of LFEs per year in each family, ~ 700 LFEs/yr. This estimate yields a total slip of ~ 0.05 mm per LFE. The slip/LFE may be overestimated if some amount of slip is accommodated aseismically [Beeler et al., 2001; Chen and Lapusta, 2009] or if the LFE catalog is incomplete [Bostock et al., 2015] and may be underestimated if LFEs within a given family do not rupture the same exact spot on the fault. Combining the 0.05 mm/event with the average of the two rise times results in a slip velocity of ~ 0.24 mm/s. While this is a low velocity, we note that Rubin [2008] and Daub et al. [2011] found that slip speeds of order 0.1 mm/s were sufficient to radiate seismically.

Using our estimates of the slip, rise time, and moment we can estimate the LFE stress drop. We do this by first defining the seismic moment as $M_o = \mu A \delta$, where μ is the rigidity, assumed to be 30 GPa, A is the slipped area, and δ is the slip. We then define the LFE asperity as having an elliptical shape with $A = \pi \gamma L^2$, where L is the short dimension and γ is the aspect ratio. The stress drop is defined as

$$\Delta\sigma \approx \frac{\mu \dot{\delta}}{2L}. \quad (1)$$

Combining the definitions of moment and area, plugging the resulting expression into equation (1), rearranging for slip, and dividing both sides by the LFE timescale results in

$$\dot{\delta} = \sqrt[3]{4M_o \Delta\sigma^2 / \mu^3 \pi \gamma} / T \quad (2)$$

where $\dot{\delta}$ is the average slip rate and T is the timescale estimated from the eGf analysis. Assuming that the moment magnitude of the LFE is ~ 1 [Hanks and Kanamori, 1979], we can create the tradeoff curve between

is consistent with estimates of instantaneous frequency of the direct S wave arrivals at some of the cleanest stations (e.g., FROB and CCRB) [see Bostock et al., 2015]. We note that any finite duration effects from the eGf could bias our estimate to be slightly shorter than the true duration. We also explored azimuthal variations in duration to determine if any directivity is present in the data (as directivity is often used to estimate the rupture extent of large earthquakes). Variability of duration was neither systematic nor significantly different from the average duration suggesting that the variations do not originate at the source. The lack of observable directivity is not surprising given the small event sizes, long durations, and use of LFE stacked waveforms in our duration analysis, which can obscure directivity signatures that may be present in individual LFE records.

Up to this point we have referred to the LFE timescale simply as a duration; however, typical earthquake source models include two characteristic timescales: the rise time (the duration of slip a point on the fault), and the rupture duration (the total amount of time it takes to rup-

average slip velocity and stress drop for an event with a rise time of 0.2 s. This tradeoff curve is shown in Figure 4a for γ between 1 and 5. A slip velocity of 0.24 mm/s suggests that the stress drop of LFEs on the San Andreas are $\sim 10^4$ Pa. This estimate is 2–3 orders of magnitude smaller than for ordinary earthquakes [Allmann and Shearer, 2007; Baltay et al., 2011] but is consistent with measured stress drops for larger slow earthquakes ranging from M 5– M 9 [Brodsky and Mori, 2007; Ito and Obara, 2006; Gao et al., 2012], and M 1–2 LFEs in Cascadia [Sweet et al., 2014; Bostock et al., 2015]. Finally, using the slip velocity of 0.24 mm/s and stress drop 10 kPa we estimate the rupture velocity, V , of 0.7 km/s using the expression $V = \mu \cdot \delta / \Delta \sigma$. This comes from taking the time derivative of equation (1). This rupture velocity is approximately 20% of the shear wave velocity β at these depths [Thurber et al., 2006], whereas typical earthquakes are thought to have rupture speeds that are 80–90% of the shear wave velocity.

4. Discussion

For small earthquakes, seismic radiation is most commonly interpreted in the context of kinematic models of the earthquake source [Madariaga, 2007]. One common attribute of a class of such models, known as omega squared models, is that their high-frequency spectra decay as ω^{-2} [Brune, 1970; Sato and Hirasawa, 1976] or ω^{-3} [Boatwright, 1980]. Zhang et al. [2011] find that LFE spectra are described by similar falloff which suggests that omega squared models may be useful in interpreting LFE spectra. Far-field S wave spectra have approximately constant amplitude at low frequency that approaches a zero frequency asymptote proportional to the seismic moment, while at high frequency the amplitude decreases with increasing frequency. The corner frequency separates these two regimes and is inversely proportional to the rupture duration. Together, the slow slip velocity, low stress drop, and slow rupture velocity can explain the depletion of high-frequency content in LFEs. Since the rupture and slip velocity of LFEs is much lower than that of ordinary earthquakes, the corner frequency shifts to lower values resulting in diminished amplitude at frequencies that exceed the LFE corner frequency (Figure 4b).

Sustained slow slip events require a mechanism that allows slip to nucleate and accelerate at low slip speeds and quench before reaching seismic slip speeds. The physical processes responsible for regulating slow slip remain a matter of debate. Models employing slip-induced dilatancy [Segall et al., 2010], a velocity weakening to strengthening transition [Shibazaki and Iio, 2003; Hawthorne and Rubin, 2013], and variable frictional properties [Ando et al., 2010; Daub et al., 2011; Skarbak et al., 2012] each appear able to reproduce first-order characteristics of slow slip events such as duration, moment, and slip speed. LFEs are often thought of as small asperities surrounded by aseismically creeping fault—they are unusual in that they produce detectable seismic waves, whereas the surrounding region that is also undergoing slip does not [Shelly et al., 2007; Beeler et al., 2013].

So what is the difference between an LFE asperity and the surrounding fault that does not radiate detectable seismic energy? The low slip velocities of LFEs we document in this study demonstrate that LFEs are regions of the fault where the slip can accelerate more than the surrounding fault, resulting in larger average slip speeds. Although slow slip has not been detected geodetically in Parkfield, the presence of occasional large LFE/tremor bursts suggests that small slow slip events do occur [Guilhem and Nadeau, 2012]. Typically, slow slip speeds are 10–100 times larger than the long-term plate slip rate; in Parkfield this corresponds to $1\text{E}-4$ to $1\text{E}-5$ mm/s. Our documented LFE slip speeds are 1000–10,000 times faster than slow slip speeds, of order 0.1 mm/s, and are barely seismic. Hence, slip speed may ultimately govern the distribution of LFE asperities in deep fault zones. This idea is qualitatively supported by the observation that some of the lowest amplitude LFE sources in Parkfield occur immediately adjacent to an ~ 10 km wide gap at the same depth as the LFEs, where no LFE sources have been detected [see Shelly and Hardebeck, 2010, Figure 1].

Finally, the observation that LFEs slip faster than typical slow slip speed but slower than regular earthquakes suggests that the same constitutive equation for fault slip may explain both the seismic and aseismic components of slow slip and that while spatial variations in bulk rheology may be present [see Fagereng et al., 2014], they are not required to produce both behaviors. As a simple example of this point, if rate and state friction with a velocity-weakening to velocity-strengthening rheology were employed as a constitutive equation for slow slip, localized regions of accelerated slip (i.e., LFEs) can be produced by spatial variations in the cutoff velocity, effective stress, or frictional parameters a and b [Hawthorne and Rubin, 2013]. These changes in constitutive parameters can be rationalized by appealing to local variations in fluid pressure and/or lithology.

5. Conclusions

We have shown that eGf analysis often applied to traditional earthquake source can also be applied to LFEs. We applied eGf analysis to two LFE families on the deep SAF and find slip durations of 0.19 and 0.22 s for the two families. Assuming that the total slip in each event is approximately the annual slip rate divided by the annual LFE rate, we calculated a slip velocity during the LFEs of ~ 0.24 mm/s, a stress drop on the order of ~ 10 kPa, and a rupture velocity of 20% of the shear wave speed, whereas traditional earthquakes have slip rates that are orders of magnitude larger, stress drops of ~ 1 MPa, and rupture velocities of 80–90% the shear wave speed. The low stress drops, slip, and propagation speeds are all lower than those of typical earthquakes of similar magnitude and suggest that the same mechanism, applied to varying extent, could be responsible for limiting slip speeds of both slow slip events and LFEs. The physical process and related properties controlling maximum slip speed remain an important topic for future investigations.

Acknowledgments

A.M.T. was supported by a National Science Foundation EAR Postdoctoral Fellowship (award ID 1249775). The Generic Mapping Tools software was used to make Figures 1 and 2 [Wessel and Smith, 2004]. Waveform data, metadata, and data products for this study were accessed through the Northern California Earthquake Data Center (NCEDC), doi:10.7932/NCEDC. HRSN stations are operated by UC-Berkeley. The authors thank Nick Beeler, Michel Bostock, Roland Bürgmann, Annemarie Baltay, and an anonymous reviewer for insightful comments on this manuscript.

References

- Abercrombie, R. E. (2015), Investigating uncertainties in empirical Green's function analysis of earthquake source parameters, *J. Geophys. Res. Solid Earth*, *120*, 4263–4277, doi:10.1002/2015JB011984.
- Allmann, B. P., and P. M. Shearer (2007), Spatial and temporal stress drop variations in small earthquakes near Parkfield, California, *J. Geophys. Res.*, *112*, B04305, doi:10.1029/2006JB004395.
- Ando, R., R. Nakata, and T. Hori (2010), A slip pulse model with fault heterogeneity for low-frequency earthquakes and tremor along plate interfaces, *Geophys. Res. Lett.*, *37*, L10310, doi:10.1029/2010GL043056.
- Baltay, A. S., S. Ide, and G. C. Beroza (2014), Radiated energy of great earthquakes from teleseismic empirical Green's function deconvolution, PAGEOPH topical edition, *Earthquake Source Phys. Various Scales*, doi:10.1007/s00024-014-0804-0.
- Baltay, A., S. Ide, G. Prieto, and G. Beroza (2011), Variability in earthquake stress drop and apparent stress, *Geophys. Res. Lett.*, *38*, L06303, doi:10.1029/2011GL046698.
- Beeler, N. M., D. A. Lockner, and S. H. Hickman (2001), A simple creep-slip and stick-slip model for repeating earthquakes and its application to micro-earthquakes at Parkfield, *Bull. Seismol. Soc. Am.*, *91*, 1797–1804.
- Beeler, N. M., A. Thomas, R. Bürgmann, and D. Shelly (2013), Inferring fault rheology from low-frequency earthquakes on the San Andreas, *J. Geophys. Res. Solid Earth*, *118*, 5976–5990, doi:10.1002/2013JB010118.
- Beroza, G. C., and S. Ide (2011), Slow earthquakes and nonvolcanic tremor, *Annu. Rev. Earth Planet. Sci.*, *39*, 271–296.
- Boatwright, J. (1980), A spectral theory for circular seismic sources; simple estimates of source dimension, dynamic stress drop, and radiated seismic energy, *Bull. Seismol. Soc. Am.*, *70*(1), 1–27.
- Bostock, M. G., A. M. Thomas, G. Savard, L. Chuang, and A. M. Rubin (2015), Magnitudes and moment-duration scaling of low-frequency earthquakes beneath southern Vancouver Island, *J. Geophys. Res. Solid Earth*, *120*, 6329–6350, doi:10.1002/2015JB012195.
- Brodsky, E. E., and J. Mori (2007), Creep events slip less than ordinary earthquakes, *Geophys. Res. Lett.*, *34*, L16309, doi:10.1029/2007GL030917.
- Brown, J. R., S. G. Prejean, G. C. Beroza, J. S. Gombert, and P. J. Haeussler (2013), Deep low-frequency earthquakes in tectonic tremor along the Alaska-Aleutian subduction zone, *J. Geophys. Res. Solid Earth*, *118*, 1079–1090, doi:10.1029/2012JB009459.
- Bruno, J. N. (1970), Tectonic stress and the spectra of seismic shear waves from earthquakes, *J. Geophys. Res.*, *75*(26), 4997–5009, doi:10.1029/JB075i026p04997.
- Chamberlain, C. J., D. R. Shelly, J. Townend, and T. A. Stern (2014), Low-frequency earthquakes reveal punctuated slow slip on the deep extent of the Alpine Fault, New Zealand, *Geochem. Geophys. Geosyst.*, *15*, 2984–2999, doi:10.1002/2014GC005436.
- Chen, T., and N. Lapusta (2009), Scaling of small repeating earthquakes explained by interaction of seismic and aseismic slip in a rate and state fault model, *J. Geophys. Res.*, *114*, B01311, doi:10.1029/2008JB005749.
- Daub, E. G., D. R. Shelly, R. A. Guyer, and P. A. Johnson (2011), Brittle and ductile friction and the physics of tectonic tremor, *Geophys. Res. Lett.*, *38*, L10301, doi:10.1029/2011GL046866.
- Dreger, D., R. M. Nadeau, and A. Chung (2007), Repeating earthquake finite source models: Strong asperities revealed on the San Andreas Fault, *Geophys. Res. Lett.*, *34*, L23302, doi:10.1029/2007GL031353.
- Fagereng, Å., G. W. B. Hillary, and J. F. A. Diener (2014), Brittle-viscous deformation, slow slip, and tremor, *Geophys. Res. Lett.*, *41*, 4159–4167, doi:10.1002/2014GL060433.
- Frank, W. B., N. M. Shapiro, V. Kostoglodov, A. L. Husker, M. Campillo, J. S. Payero, and G. A. Prieto (2013), Low-frequency earthquakes in the Mexican Sweet Spot, *Geophys. Res. Lett.*, *40*, 2661–2666, doi:10.1002/grl.50561.
- Gao, H., D. A. Schmidt, and R. J. Weldon (2012), Scaling relationships of source parameters for slow slip events, *Bull. Seismol. Soc. Am.*, *102*(1), 352–360.
- Guilhem, A., and R. M. Nadeau (2012), Episodic tremors and deep slow-slip events in Central California, *Earth Planet. Sci. Lett.*, *357*, 1–10.
- Hanks, T. C., and H. Kanamori (1979), A moment magnitude scale, *J. Geophys. Res.*, *84*(B5), 2348–2350, doi:10.1029/JB084iB05p02348.
- Hartzell, S. H. (1978), Earthquake aftershocks as Green's functions, *Geophys. Res. Lett.*, *5*(1), 1–4, doi:10.1029/GL005i001p00001.
- Hawthorne, J. C., and A. M. Rubin (2013), Laterally propagating slow slip events in a rate and state friction model with a velocity-weakening to velocity-strengthening transition, *J. Geophys. Res. Solid Earth*, *118*, 3785–3808, doi:10.1002/jgrb.50261.
- Ide, S., et al. (2007a), A scaling law for slow earthquakes, *Nature*, *447*(7140), 76–79.
- Ide, S., D. R. Shelly, and G. C. Beroza (2007b), Mechanism of deep low frequency earthquakes: Further evidence that deep non-volcanic tremor is generated by shear slip on the plate interface, *Geophys. Res. Lett.*, *34*, L03308, doi:10.1029/2006GL028890.
- Ito, Y., and K. Obara (2006), Very low frequency earthquakes within accretionary prisms are very low stress-drop earthquakes, *Geophys. Res. Lett.*, *33*, L09302, doi:10.1029/2006GL025883.
- Madariaga, R. (2007), Seismic source theory, *Treatise on Geophysics*, *4*, 59–82.
- Mueller, C. S. (1985), Source pulse enhancement by deconvolution of an empirical Green's function, *Geophys. Res. Lett.*, *12*(1), 33–36, doi:10.1029/GL012i001p00033.
- Plourde, A. P., M. G. Bostock, P. Audet, and A. M. Thomas (2015), Low-frequency earthquakes at the southern Cascadia margin, *Geophys. Res. Lett.*, *42*, 4849–4855, doi:10.1002/2015GL064363.

- Royer, A. A., and M. G. Bostock (2014), A comparative study of low frequency earthquake templates in northern Cascadia, *Earth Planet. Sci. Lett.*, *402*, 247–256.
- Rubin, A. M. (2008), Episodic slow slip events and rate-and-state friction, *J. Geophys. Res.*, *113*, B11414, doi:10.1029/2008JB005642.
- Ryder, I., and R. Bürgmann (2008), Spatial variations in slip deficit on the central San Andreas fault from InSAR, *Geophys. J. Int.*, *175*(3), 837–852.
- Sato, T., and T. Hirasawa (1973), Body wave spectra from propagating shear cracks, *J. Phys. Earth*, *21*(4), 415–431.
- Segall, P., A. M. Rubin, A. M. Bradley, and J. R. Rice (2010), Dilatant strengthening as a mechanism for slow slip events, *J. Geophys. Res.*, *115*, B12305, doi:10.1029/2010JB007449.
- Shelly, D. R., and J. L. Hardebeck (2010), Precise tremor source locations and amplitude variations along the lower-crustal central San Andreas Fault, *Geophys. Res. Lett.*, *37*, L14301, doi:10.1029/2010GL043672.
- Shelly, D. R., G. C. Beroza, and S. Ide (2007), Non-volcanic tremor and low-frequency earthquake swarms, *Nature*, *446*(7133), 305–307.
- Shibasaki, B., and Y. Iio (2003), On the physical mechanism of silent slip events along the deeper part of the seismogenic zone, *Geophys. Res. Lett.*, *30*(9), 1489, doi:10.1029/2003GL017047.
- Skarbek, R. M., A. W. Rempel, and D. A. Schmidt (2012), Geologic heterogeneity can produce aseismic slip transients, *Geophys. Res. Lett.*, *39*, L21306, doi:10.1029/2012GL053762.
- Sweet, J. R., K. C. Creager, and H. Houston (2014), A family of repeating low-frequency earthquakes at the downdip edge of tremor and slip, *Geochem. Geophys. Geosyst.*, *15*, 3713–3721, doi:10.1002/2014GC005449.
- Thomas, A. M., and M. G. Bostock (2015), Identifying low-frequency earthquakes in central Cascadia using cross-station correlation, *Tectonophysics*, *658*, 111–116.
- Thomas, A. M., R. Bürgmann, D. R. Shelly, N. M. Beeler, and M. L. Rudolph (2012), Tidal triggering of low frequency earthquakes near Parkfield, California: Implications for fault mechanics within the brittle-ductile transition, *J. Geophys. Res.*, *117*, B05301, doi:10.1029/2011JB009036.
- Thurber, C., S. Roecker, H. Zhang, S. Baher, and W. Ellsworth (2004), Fine-scale structure of the San Andreas Fault and location of the SAFOD target earthquakes, *Geophys. Res. Lett.*, *31*, L12502, doi:10.1029/2003GL019398.
- Thurber, C., H. Zhang, F. Waldhauser, J. Hardebeck, A. Michael, and D. Eberhart-Phillips (2006), Three-dimensional compressional wave speed model, earthquake relocations, and focal mechanisms for the Parkfield, California, region, *Bull. Seismol. Soc. Am.*, *96*(4B), S38–S49.
- Waldhauser, F., and D. P. Schaff (2008), Large-scale relocation of two decades of Northern California seismicity using cross-correlation and double-difference methods, *J. Geophys. Res.*, *113*, B08311, doi:10.1029/2007JB005479.
- Wessel, P., and W. H. F. Smith (2001), The generic mapping tools, 2013-01-01. [Available at <http://gmt.soest.hawaii.edu>.]
- Zhang, J., P. Gerstoft, P. M. Shearer, H. Yao, J. E. Vidale, H. Houston, and A. Ghosh (2011), Cascadia tremor spectra: Low corner frequencies and earthquake-like high-frequency falloff, *Geochem. Geophys. Geosyst.*, *12*, Q10007, doi:10.1029/2011GC003759.